International Journal of Innovative
Computing, Information and Control
Volume **15**, Number **1**, February **2019**

ICIC International ©2019 ISSN 1349-4198
pp. **275–289**

CONTROL ANALYSIS OF THE HYDRAULIC LUFFING SYSTEM CONTROLLED BY THE NEW HYDRAULIC TRANSFORMER FOR RESCUE VEHICLES

Zhiqiang Chao, Chuming Ning, Huaying Li and Shousong Han

Department of Vehicle Engineering
Academy of Army Armored Force
No. 21, Dujiakan, Fengtai District, Beijing 100072, P. R. China
ncm20081273@126.com

Received March 2018; revised July 2018

Abstract. *On account of the high energy consumption and low energy utilization rate of valve-controlled hydraulic luffing systems for rescue vehicles and their susceptibility to the problems of relatively significant instantaneous pressure impact and speed fluctuations, a new hydraulic luffing system adopting a new type hydraulic transformer for hydraulic cylinder control has been designed in this paper. First, an experiment on the performance of the valve-controlled system was conducted, and then its control performance and energy consumption were analyzed. The structure and working principle of the new hydraulic luffing system was then analyzed, and a mathematical model of the system was built. A control strategy, combining the switching preset control angle and a fuzzy PID controller, has been proposed to improve the smoothness of the switching process. And then the control performance and energy consumption of the new system were investigated. As shown in the results, the new hydraulic luffing system could track the input speed well and it did not show any intense pressure or flow oscillation, which meant that the system demonstrated good control performance. Compared to the valve-controlled hydraulic luffing system, the new system was characterized by an obvious energy-saving effect and a significantly improved energy utilization rate.*

Keywords: Hydraulic transformer, Luffing system, Switching preset control angle, Fuzzy PID

1. **Introduction.** The hydraulic luffing system used in rescue vehicles is a manual multi-way valve-controlled system that mainly plays the roles of quickly lifting/descending and supporting the hoisting device of rescue vehicles. Due to the relatively significant overflow loss from the relief valve, the bypass throttling loss from the multi-way valve and other forms of energy losses during the service process, the system has an extremely low energy utilization rate. Moreover, because of the extremely strong nonlinearity of the hydraulic luffing system, the uncertainty of internal parameters and the relatively frequent and intense changes of load, the valve-controlled hydraulic system is extremely susceptible to relatively significant instantaneous pressure impacts and speed fluctuations. Therefore, some improving measures are needed for the valve-controlled hydraulic luffing systems, which will reduce its energy consumption, increase its energy utilization rate and improve the control quality.

The secondary regulation system of the Common Pressure Rail (CPR) is a control system that uses secondary elements to regulate the pressure, flow and other parameters of the controlled object under constant pressure. It can independently connect several unrelated loads in parallel onto the same CPR, thus effectively avoiding flow coupling

DOI: 10.24507/ijicic.15.01.275

in the hydraulic system and improving its efficiency [1-4]. In recent years, the hydraulic energy-saving technology that has adopted CPR as the energy source and uses a Hydraulic Transformer (HT) for the secondary regulation of pressure and flow has proven to be fruitful in terms of reducing the system's energy consumption, increasing its energy utilization rate, improving its control performance and so forth [5-7].

The Innas Hydraulic Transformer (IHT) [8] with three distributing launders, is proposed for the first time by Innas (Netherlands) in 1997. The transformation ratio, between the oil source and the load can be quick adjusted by changing the rotational angle of the port plate. And the IHT was used to establish a hydraulic hybrid system with a hydraulic accumulator, and the hydraulic hybrid system can recycle and reuse energy. However, given that it achieves voltage transformation through manually regulating the angle of the port plate, it is difficult for it to achieve automatic control of variable-load conditions. A self-adaptive system, controlled by hydraulic transformer, for the hydraulic hybrid vehicle was presented by Wu et al. [9], and it had a higher reliability and a lower cost, compared with the convention electric-hydraulic system. The configuration mode of a CPR-based hydraulic hybrid excavator, adopted in [10], used an SHT to conduct secondary regulation and control over the hydraulic cylinder and eliminate the throttling loss of the system. A power take-off concept for wave energy converters based on oil-hydraulic transformer units was proposed [11], which achieved good energy-saving effect.

The secondary regulation system that has adopted an HT for pressure and flow control can also relatively satisfactorily reduce the system's energy consumption and increase its energy utilization rate, but suitable control algorithms are needed to improve the control performance of the various control systems in multi-working conditions and variable-load environments [12-14]. The adaptive robust control [15], the sliding adaptive control [16], and other control methods based on the adaptive control theory [17] have realized fine control over the nonlinear and parametric uncertainties of the electro-hydraulic servo system, and have been successfully applied to spacecraft control, engineering vehicles and many other fields [18,19].

Some effective control algorithms combined with modern control theory had been used to improve the dynamic performance of system; for example, a control strategy combining dynamic pressure feedback and adaptive fuzzy control was used to solve the problem of the "downward movement" of the mechanical arm in the initial period of adopting an SHT to control hydraulic cylinder movement [20,21].

This paper presented a new hydraulic luffing system for rescue vehicles adopting an SHT for hydraulic cylinder control with a CPR. And then a control strategy, switching preset control angle, was presented for the speed control of hydraulic cylinder of new system. The performance comparison between the valve-controlled hydraulic system and the new hydraulic luffing system was also provided. It was aimed to effectively reduce the energy consumption of the hydraulic luffing system for rescue vehicles and improve its control performance.

2. Experiment on the Valve-Controlled Hydraulic System.

In order to obtain the speed, pressure and other parameters of the hydraulic cylinder during actual operation of rescue vehicles and to ensure that the proposed new SHT-controlled luffing system could match actual working conditions, the displacement, flow, pressure and other data of the rescue vehicle during no-load service were collected in this paper. When analyzing the performance of the new system, the same working cycle completing the actions of hydraulic cylinder control was adopted. Thus, although they had different configurations and control modes, the two systems nevertheless presented basically consistent speed change trends under no-load working conditions, so the measured speed data was used as

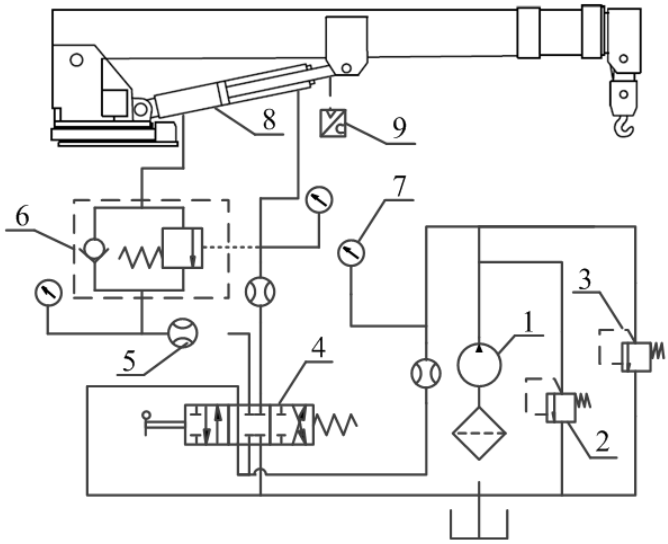

1. Fixed displacement pump, 2&3. Relief valve, 4. Multi-way valve, 5. Flow sensor
6. Balance valve, 7. Pressure sensor, 8. Hydraulic cylinder, 9. Displacement sensor

FIGURE 1. Schematic diagram of the valve-controlled hydraulic luffing system

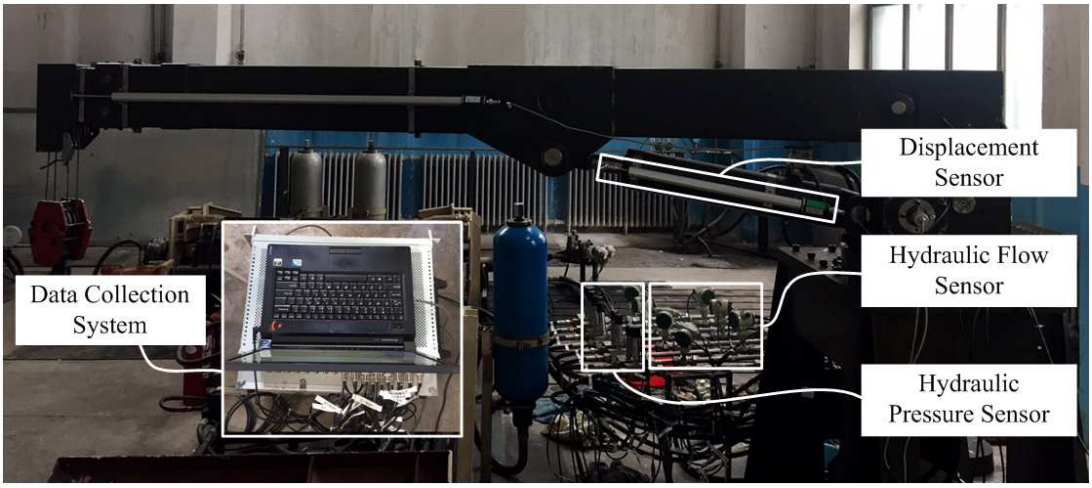

FIGURE 2. Structure of the experimental system

the input signal of the new system to analyze the performance of the new system in this paper.

Figure 1 depicts the schematic diagram of the valve-controlled hydraulic luffing system. The system was mainly composed of a fixed displacement pump, a manual multi-way valve, a balance valve, a relief valve, a hydraulic cylinder, etc. The opening pressures of relief valve 2 and relief valve 3 were 7MPa and 11MPa respectively; the pipeline between relief valve 2 and the multi-way valve was relatively complex, with a relatively significant pressure loss.

According to the layout of the various sensors in Figure 1, the structure of the experimental system of the valve-controlled system was built as Figure 2. Then the sampling frequency was set to be 200Hz. Given that what was collected by the experimental system was the displacement signal of the hydraulic cylinder, and that this paper adopted the speed signal as its main object of analysis, first differential processing was used on the displacement signal, and then a low-pass filter with a frequency of 8Hz was used for the

TABLE 1. The parameters of the experimental system's main components

Component	Output Signal	Rang
Hydraulic pressure	0-5V	0-15MPa
Hydraulic flow	1-5V	20/3-400/3L/min
Cylinder displacement of the luffing system	0-10V	0-500mm

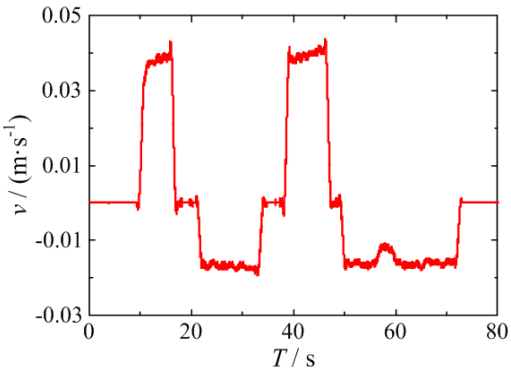

FIGURE 3. Speed curve of hydraulic cylinder

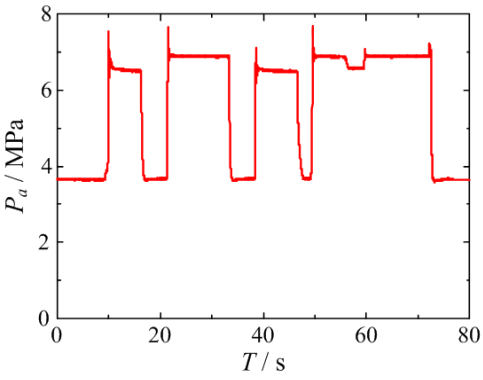

FIGURE 4. Pressure curve of main oil passage

filter processing of the signal, thus obtaining the running speed of the hydraulic cylinder. The parameters of the experimental system's main components can be seen in Table 1.

Figure 3 depicts the speed of the hydraulic cylinder during two cycles. Figure 4 depicts the pressure of the main oil passage close to the multi-way valve. As can be seen from these figures there were relatively significant pressure fluctuations at the instant of opening/closing the multi-way valve, and the speed of the system showed an obvious oscillation, and the change in the speed was frequent and intense. And the main reason was that, the external interferences caused by the hook swing and other factors resulted in intense load fluctuations, while the hydraulic system, controlled by the manual multi-way valve, could not effectively and quickly adjust the system pressure to adapt to such fluctuations, so the hydraulic cylinder experienced intense speed fluctuations.

Figure 5 depicts the power curves of various major parts of the valve-controlled system; Figure 6 depicts the energy consumption of various major parts of the valve-controlled system. As can be seen from Figure 5, when the multi-way valve was placed in the neutral position, that is, when the system was not activated, the total power consumption of the system was about 3kW, and the power consumption of the multi-way valve accounted for the majority of the system's energy consumption; when the multi-way valve was placed in the left or right position, that is, when the system was completing the action of lifting the arm or lowering the arm, the total power consumption of the system was about 5kW. A large amount of energy was consumed by the relief valve, and the power used for the hydraulic cylinder to complete the actions of lifting the arm and lowering the arm did not exceed 2kW at any point. According to Figure 6, the energy consumed by the multi-way valve and the relief valve accounted for the majority (88.19%) of the hydraulic system's energy consumption, while the effective energy consumed by the hydraulic cylinder in completing the action of lifting the arm or lowering the arm only accounted for 11.82%. Thus, it was necessary to introduce corresponding measures to reduce the energy consumption of the multi-way valve and the relief valve, thus lowering the system's energy consumption and increasing its energy utilization rate.

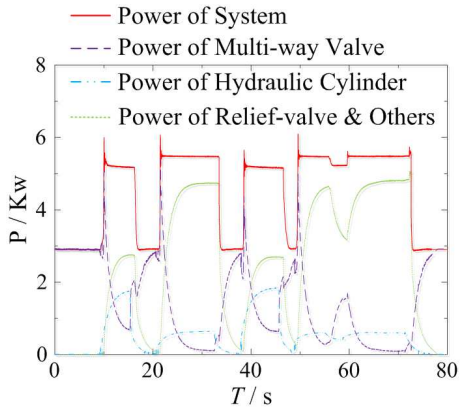

FIGURE 5. Power curves of various major parts of the valve-controlled system

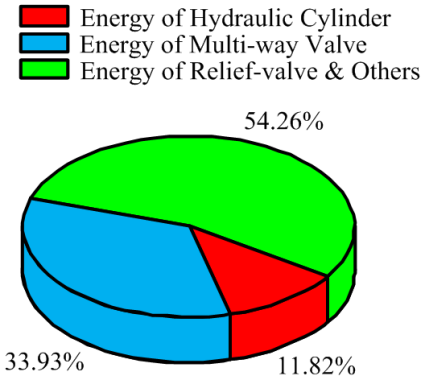

FIGURE 6. Energy consumption of various major parts of valve-controlled system

3. **Structure and Working Principle of the New Hydraulic Luffing System.** The valve-controlled hydraulic system was an open throttle system, so throttling loss was inevitable and the operability and stability are relatively poor. In order to enhance the steadiness and smoothness of the arm rising and descending, and significantly reduce the system's energy consumption and increase its energy utilization rate, this paper has proposed a new hydraulic luffing system for rescue vehicles adopting an SHT for hydraulic cylinder control. The new hydraulic luffing system for rescue vehicles has adopted the control mode of the power source-SHT-luffing mechanism; the structural principle of the system is shown in Figure 7. The entire hydraulic luffing system is composed of a CPR, SHT, pilot control system, high-speed switch valve, hydraulic cylinder, etc. The CPR further consists of a constant high-pressure circuit and a low-pressure circuit, the former of which was supplied by a constant pressure variable pump and a hydraulic accumulator, the latter of which was directly connected with the oil tank. The oil of the high-pressure circuit, after being regulated by the SHT, acted on the head port of the hydraulic cylinder to adapt to the demand of the changing load. Compared with the valve-controlled hydraulic system, the new hydraulic luffing system used the hydraulic accumulator as the energy storage, which can recycle the gravitational potential energy of hydraulic cylinder during the descending process and reduce the calorific value of the system. Using SHT as the control component can realize relatively precision quantitative control of hydraulic cylinder, and then improve system efficiency.

The SHT was integrated with the pilot control system which exerted precise angular displacement control of the port plate over the angle δ [22,23]. The structural schematic diagram of the pilot control system composed of the swing motor and electro-hydraulic servo valve can be seen in Figure 8. This was different from the two-port port plate of the traditional hydraulic pump/motor, the port plate of the SHT had three ports, port A, port B, and port T (as shown in section in Figure 9), which were connected with the CPR high-pressure circuit, the hydraulic cylinder's head port, and the oil return tank respectively. The rotational direction and speed of the SHT cylinder were mainly determined by the sum of the torque values of the three ports.

During the arm lifting process of the hydraulic cylinder, the high-speed quick-closing valves V2 and V3 were opened, and V1 operated under left-position condition. In this case, oil first went through the high-pressure pipeline of the CPR system, and was then supplied to hydraulic cylinder's head port via the load port of the SHT, thus causing the hydraulic cylinder to rise up. The functional diagram of system arm rising can be

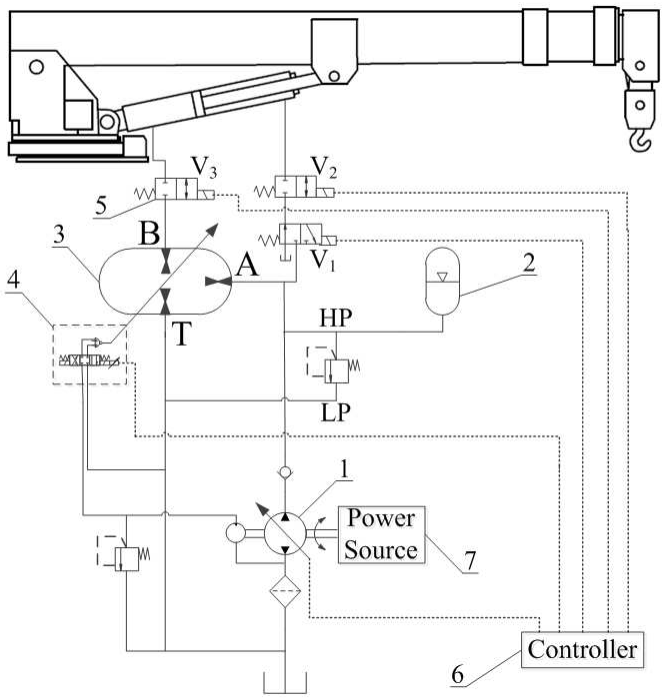

1. Constant pressure variable pump, 2. Hydraulic accumulator, 3. SHT, 4. Pilot control system
5. Solenoid directional control valve, 6. Controller, 7. Power source

FIGURE 7. Structural schematic diagram of the new hydraulic luffing system

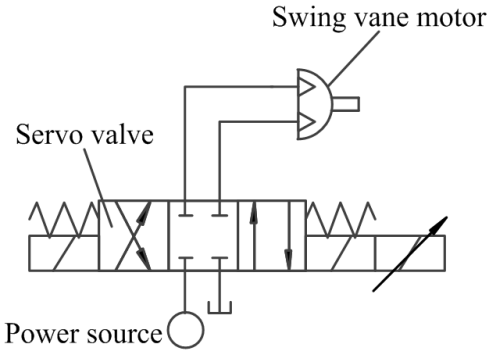

FIGURE 8. Structural schematic diagram of the pilot control system

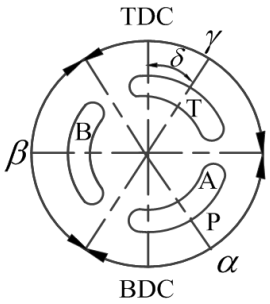

FIGURE 9. The section of port plate of SHT

seen in Figure 10. During the arm descending process of the hydraulic cylinder, the high-speed quick-closing valves V2 and V3 were opened, and V1 operated under right-position condition. In this case, the hydraulic cylinder's rod port was directly connected with the high-pressure pipeline, and the hydraulic cylinder moved downwards under the force of gravity and the high-pressure oil from the rod port, and the hydraulic accumulator was used to realize energy recovery. The functional diagram of the system arm descending can be seen in Figure 11.

4. **Mathematical Model.** The mathematical model for the dynamic conversion of the force of the hydraulic cylinder is [20]

$$P_B \cdot A_2 - P_A \cdot A_1 = m \cdot \ddot{s} + B_d \cdot \dot{s} + K \cdot s + m \cdot g + F_f + F_d \tag{1}$$

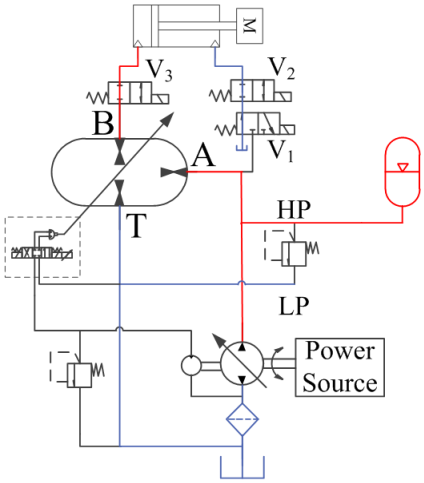

FIGURE 10. Functional diagram of the system arm lifting process

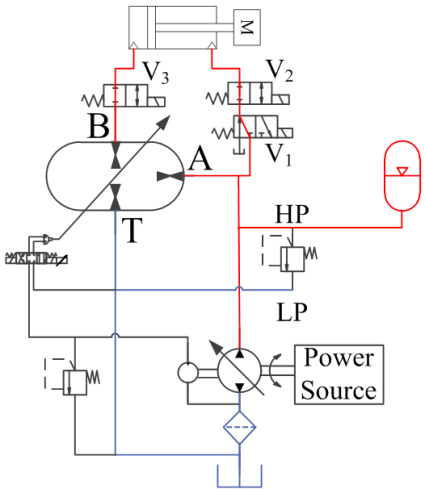

FIGURE 11. Functional diagram of the system arm descending process

During the system arm lifting process, valve V1's control signal $x_{V1} = 0$; during the system arm descending process, valve V1's control signal $x_{V1} = 1$; then the flow into the hydraulic cylinder's head port and the flow out of its rod port respectively were

$$q_{db} = A_2 \cdot \dot{s} + \frac{V_2}{\beta_e} \cdot \frac{dP_B}{dt} + C_{ic}(P_B - P_A) + C_{ec} \cdot P_B \tag{2}$$

$$q_{dr} = A_1 \cdot \dot{s} - \frac{V_1}{b_e} \cdot \frac{dP_1}{dt} - C_{ic}(P_1 - P_B) - C_{ec} \cdot P_1 \tag{3}$$

$$P_1 = \begin{cases} 0 & x_{V1} = 0 \\ P_A & x_{V1} = 1 \end{cases} \tag{4}$$

wherein A_1 represents the area of the hydraulic cylinder's rod port; A_2 represents the area of the hydraulic cylinder's head port; m represents the load mass; s represents the displacement of the hydraulic cylinder; B_d represents the viscous damping coefficient; K represents the elastic coefficient; F_f represents the frictional force; F_d represents the external load force; C_{ic} represents the internal leakage coefficient; and C_{ec} represents the external leakage coefficient.

The rotation of the SHT cylinder mainly depended on the sum of the torque values of the port plate's three ports; the torque models for the three oil ports and their sum of torques respectively were

$$T_i = \frac{P_i \cdot V_{HT}}{2\pi} \cdot \sin\frac{\alpha}{2} \cdot \chi \tag{5}$$

$$\Delta T = J_{HT} \cdot \dot{\omega}_{HT} = \sum_i T_i \tag{6}$$

$$\chi = \begin{cases} \sin\delta & i = A \\ \sin\left(\delta - \dfrac{\alpha}{2} - \dfrac{\beta}{2}\right) & i = B \\ \sin\left(\delta + \dfrac{\alpha}{2} + \dfrac{\gamma}{2}\right) & i = C \end{cases} \tag{7}$$

wherein V_{HT} represents the displacement of the SHT; P_i represents the pressure of port A\B\T; α, β, and γ represent the angles corresponding to ports A\B\T respectively; J_{HT} represents the rotational inertia of the SHT-related module; ω_{HT} represents the rotational angular speed; δ represents the control angle of the SHT's port plate.

The flows of the ports A and B of SHT respectively were [5]

$$q_A = \frac{\omega_{HT} \cdot V_{HT}}{2\pi} \cdot \sin\frac{\alpha}{2} \cdot \sin\delta + C_{im}\left(P_A - P_B\right) + C_{im}\left(P_A - P_T\right) + C_{em} \cdot P_A \tag{8}$$

$$q_B = \frac{\omega_{HT} \cdot V_{HT}}{2\pi} \cdot \sin\frac{\beta}{2} \cdot \sin\left(\delta - \frac{\alpha}{2} - \frac{\beta}{2}\right) - C_{im}\left(P_B - P_A\right) - C_{im}\left(P_B - P_T\right) - C_{em} \cdot P_B \tag{9}$$

wherein C_{im} represents the internal leakage coefficient of the SHT; C_{em} represents the external leakage coefficient of the SHT.

Regardless of the influence of the compressibility of the oil volume, considering that the hydraulic cylinder's head port was directly connected with the port B of the SHT, then the relational expression of Formula (10) could be obtained

$$q_{db} = q_B \tag{10}$$

Assuming that the oil return pressure of the swing motor was 0, then the mathematical model for the dynamic control of the pilot control system's electro-hydraulic servo valve and the mathematical model for the dynamic conversion of the swing motor's torque would respectively be

$$K_q \cdot i - K_c \cdot P_{kz} = D_m \cdot \dot{\delta} + C_m \cdot P_{kz} + \frac{V_{0\_z}}{4 \cdot \beta_e} \cdot \dot{P}_{kz} \tag{11}$$

$$D_m \cdot P_{kz} = J_m \cdot \ddot{\delta} + B_m \cdot \dot{\delta} + K_m \cdot \delta + T_t \tag{12}$$

wherein K_q represents the flow gain of the electro-hydraulic servo valve; i represents the control current of the electro-hydraulic servo valve; K_c represents the flow-pressure coefficient of the electro-hydraulic servo valve; P_{kz} represents the pressure of the swing motor's high-pressure chamber; D_m represents the displacement of the swing motor; δ represents the rotational angle of the swing motor; C_m represents the leakage coefficient of the swing motor; β_e represents the bulk modulus of elasticity; V_{0_z} represents the sum of the swing motor's initial volume and the pipeline volume; J_m represents the rotational inertia of the port plate; B_m represents the viscous damping coefficient; K_m represents the elastic coefficient; T_t represents the external load torque.

The pressure of the CPR system's high-pressure circuit was subject to restrictions by the constant pressure variable pump, the SHT, the hydraulic accumulator, and many other factors. The mathematical model for the pressure of the CPR system's high-pressure pipeline was

$$\dot{P}_A = \frac{q_p + q_{d\_r} - q_A}{\frac{1}{\beta_e}\left[V_{1\_a} + A_1 \cdot (H - s)\right] + C_{accu}} \tag{13}$$

wherein q_{d_r} represents the input flow of the hydraulic cylinder; q_p represents the output flow of the constant pressure variable pump; V_{1_a} represents the volume of the pipeline from the SHT's port A to the hydraulic cylinder's rod port; H represents the maximum stroke of the hydraulic cylinder; C_{accu} represents the oil volume of the hydraulic accumulator [25].

Assume that the pressure of the SHT's port T was 0, and that the selected state variable was

$$\mathbf{x} = \begin{bmatrix} x_1 & x_2 & x_3 & x_4 & x_5 & x_6 \end{bmatrix} = \begin{bmatrix} \delta & \omega_{HT} & P_A & P_B & s & \dot{s} \end{bmatrix} \tag{14}$$

Through rearrangement and simplification, we can obtain the state equation of the system:

$$\begin{cases} \dot{\mathbf{x}} = \begin{bmatrix} \dot{x}_1 \\ \dot{x}_2 \\ \dot{x}_3 \\ \dot{x}_4 \\ \dot{x}_5 \\ \dot{x}_6 \end{bmatrix} = \begin{bmatrix} \frac{D_m \cdot P_k - T_t - K_m \cdot x_1 + J_m \cdot \ddot{x}_1}{B_m} \\ \frac{x_2 \cdot V_{HT}}{2\pi \cdot J_{HT}} \cdot \sin\frac{\alpha}{2} \cdot \sin\delta + \frac{x_3 \cdot V_{HT}}{2\pi \cdot J_{HT}} \cdot \sin\frac{\beta}{2} \cdot \sin\left(\delta - \frac{\alpha}{2} - \frac{\beta}{2}\right) \\ \frac{-\frac{x_1 \cdot V_{HT}}{2\pi \cdot J_{HT}} \cdot \sin\frac{\alpha}{2} \cdot \sin\delta - (2C_{im} + C_{em} + C_{ic}) \cdot x_2 + (C_{im} + C_{ic}) \cdot x_3 + A_1 \cdot x_5 + q_p}{\frac{V_0}{n} \cdot \left(\frac{p_0}{x_2^{n+1}}\right)^{\frac{1}{n}} + \frac{1}{\beta_e}[V_{1\_a} + A_1 \cdot (H - x_4)]} \\ \frac{\frac{x_1 \cdot V_{HT}}{2\pi \cdot J_{HT}} \cdot \sin\frac{\beta}{2} \cdot \frac{x_1 \cdot V_{HT}}{2\pi \cdot J_{HT}} \cdot \sin\frac{\alpha}{2} + (C_{im} + C_{ic}) \cdot x_2 - (2C_{im} + C_{em} + C_{ic}) \cdot x_3 - A_2 \cdot x_5}{\frac{1}{\beta_e}[V_{1\_b} + A_2 \cdot x_4]} \\ x_5 \\ \frac{x_3 \cdot A_2 - x_2 \cdot A_1 - B_d \cdot x_5 - K \cdot x_4 - m \cdot g - F_f - F_d}{m} \end{bmatrix} \\ y = \begin{bmatrix} 0 & 0 & 0 & 0 & 0 & 1 \end{bmatrix} \mathbf{x} \end{cases} \tag{15}$$

5. **Control Strategy.** During the arm lifting and arm descending process of the luffing system, the hydraulic cylinder's rod port was connected with the oil tank and the high-pressure circuit of the CPR system respectively, and the rod port experienced a relatively significant pressure change. To adapt to such a dramatic change in the pressure of the rod port, it was necessary to quickly regulate the pressure of the head port connected with the SHT's port B. Thus, to reduce the impact of the instantaneous dramatic pressure fluctuations, caused by the transition in the operation state, on the system and improve the smoothness of the system's switching control process, this paper has proposed a control strategy for the switching preset control angle based on the input signal and pressure feedback. The switching preset control angle was the control angle δ_0 pre-regulated by the SHT's port plate. That is, before opening the high-speed switch valve and connecting the hydraulic system, the input signal of the system was used to judge the transition of its follow-up operation state, i.e., judge whether to switch to the arm lifting or arm descending process; after that, combined with the system pressure, the electro-hydraulic servo valve was used to control the rotation of the swing motor and pre-regulate the angle of the SHT's port plate to δ_0. After the system reached the switching preset control angle, the corresponding high-speed quick-closing valve was opened to connect the hydraulic system and realize the steady transition of the system operation state. As can be known from the spatial state Equation (15), the new hydraulic luffing system was not only a single-input/output system, but also a strongly nonlinear and strongly coupled time-varying system, which meant that it was very difficult to linearize from the change of angle of the SHT's port plate to the change of speed of hydraulic cylinder with the method of modern control theory. In order to avoid the decoupling analysis of the multi-control variables of the system, strengthen the robustness of the system and improve its fault tolerance, this paper regarded the system model as a "black box" and then adopted the FPID control method, a method which not only does not have to take precise mathematical models into consideration but can also utilize errors for quick parameter adjustment, in order to control the speed of the hydraulic luffing system. The control principle of the new hydraulic system can be seen in Figure 12.

An FPID controller [21,25-27] mainly consists of a fuzzy controller and a PID controller. During system operation, through continuously detecting the deviation e and the deviation change rate ec, and continuously regulating the three quantization factors ΔK_p, ΔK_i, and ΔK_d, the setting parameters could be obtained in combination with the initial PID

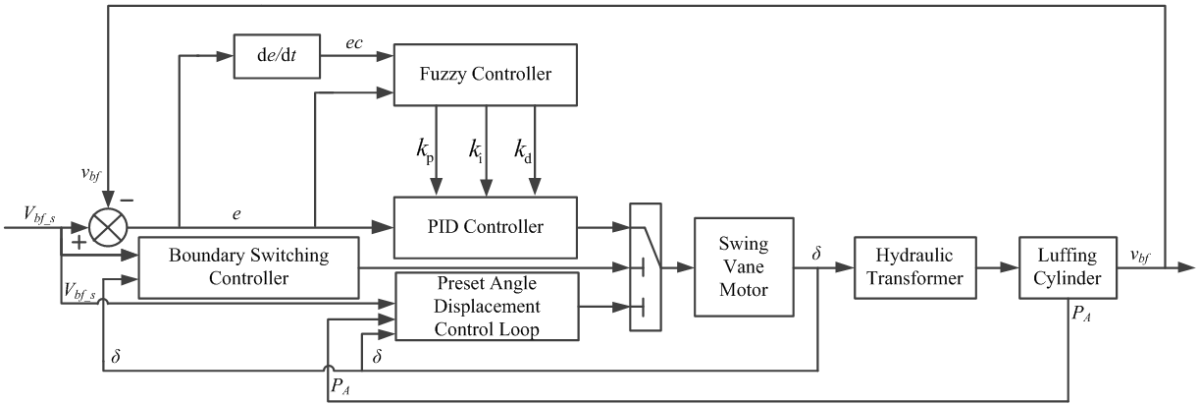

FIGURE 12. Control principle of the new hydraulic system

parameter

$$\begin{aligned} K_p &= K_{p0} + \Delta K_p \\ K_i &= K_{i0} + \Delta K_i \\ K_d &= K_{d0} + \Delta K_d \end{aligned} \tag{16}$$

In order to obtain the membership functions of fuzzy subset, the factors e, ec, ΔK_p, ΔK_i, and ΔK_d should follow a normal distribution, and then a lot of simulation analysis was performed on different PID values. At last the membership assignment table fuzzy subset and fuzzy domain were derived based on a lot of simulation analysis with different PID values. The fuzzy domain and fuzzy subset defining the input variable of the fuzzy control system are provided by Formulas (17) and (18) respectively. The elements of the fuzzy subset are represented as "negatively large", "negatively medium", "negatively small", "positively small", "positively medium", and "positively large" respectively. The membership functions of e and ec can be seen in Figure 13. The fuzzy domains of the quantization factors ΔK_p, ΔK_i, and ΔK_d are defined by Formulas (19), (20) and (21) respectively. Their membership functions can be seen in Figure 14.

$$e, ec = \{ \ -0.02 \quad -0.01 \quad -0.005 \quad 0 \quad 0.005 \quad 0.01 \quad 0.02 \ \} \tag{17}$$

$$e, ec = \{ \ NB \quad NM \quad NS \quad ZO \quad PS \quad PM \quad PB \ \} \tag{18}$$

$$\Delta K_p = \{ \ -0.1 \quad -0.06 \quad -0.02 \quad 0 \quad 0.02 \quad 0.06 \quad 0.1 \ \} \tag{19}$$

$$\Delta K_i = \{ \ -0.01 \quad -0.006 \quad -0.002 \quad 0 \quad 0.002 \quad 0.006 \quad 0.01 \ \} \tag{20}$$

$$\Delta K_d = \{ \ -0.01 \quad -0.006 \quad -0.002 \quad 0 \quad 0.002 \quad 0.006 \quad 0.01 \ \} \tag{21}$$

The fuzzy rule serves as the core of the fuzzy controller. In this paper, the relations among the various PID variable parameters were analyzed to obtain the fuzzy rule governing the regulation and modification of the PID regulator.

The result of fuzzy reasoning is the output variable of the fuzzy controller. Generally, it is a fuzzy set that cannot be directly used to control the controlled object, and it is necessary to first convert it into a precise quantity that can be executed by the actuator. This paper adopted the center of area method and utilized the degree of membership information of each element in the output domain, its precision results were relatively smooth; the center z^* of the area covered by the degree of membership $\mu_C(z)$ function of the fuzzy set C was

$$z^* = \frac{\int_a^b z \cdot \mu_C(z) dz}{\int_a^b \mu_C(z) dz}, \quad U = [a, b] \tag{22}$$

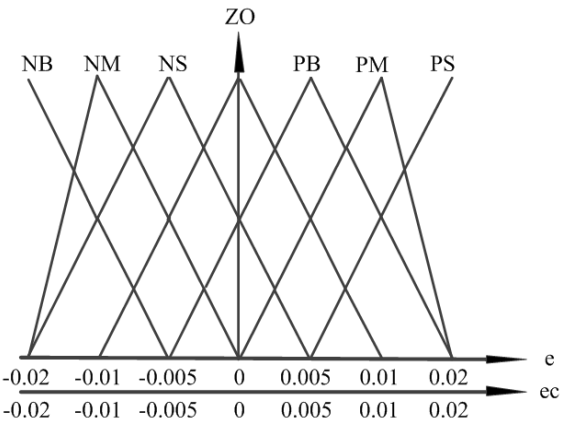

FIGURE 13. Membership functions of e and ec

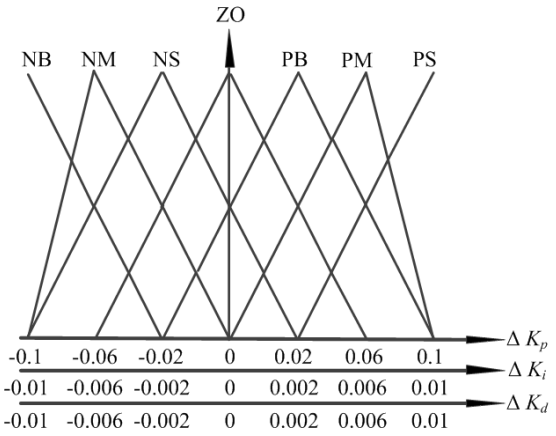

FIGURE 14. Membership functions of ΔK_p, ΔK_i, and ΔK_d

TABLE 2. Fuzzy rule table of ΔK_p, ΔK_i, and ΔK_d

e	ec						
	NB	NM	NS	ZO	PS	PM	PB
NB	NS/PS/NB	NS/PS/NB	NM/PS/ZO	NM/PM/ZO	NB/PM/ZO	NB/ZO/NS	ZO/ZO/NS
NM	NS/PS/PB	NS/PS/PB	NM/PM/PB	NM/PM/PB	NB/PB/ZO	ZO/ZO/NB	ZO/ZO/NM
NS	NM/PM/PS	NM/PM/PS	NM/PB/PM	NB/PB/PB	ZO/ZO/ZO	PB/NB/NB	PM/NB/NM
ZO	NM/PM/PS	NB/PB/PM	NB/PB/PM	ZO/ZO/PB	PB/NB/ZO	PM/NB/NB	PM/NM/NM
PS	NB/PB/PS	NB/PB/PM	ZO/ZO/PB	PB/NB/PB	PB/NB/ZO	PM/NM/NB	PM/NM/NB
PM	ZO/ZO/PM	ZO/ZO/PB	PB/NB/PB	PM/NM/PB	PM/NM/ZO	PM/NS/NB	PS/NS/NB
PB	ZO/ZO/PB	PB/ZO/ZO	PB/NB/ZO	PM/NM/ZO	PM/NS/ZO	PS/NS/NS	PS/NS/NS

TABLE 3. The parameters of main components of the new hydraulic luffing system

Component	Parameter	Value	Unit
Main pump	D_p	63	ml/r
SHT	V_{HT}	71	ml/r
Hydraulic accumulator	V_0	10	ml
	p_0	3	MPa
Swing vane motor	D_m	25	ml/r

6. **Simulation Analysis.** Based on the aforementioned mathematical model and the control strategy, a systemic simulation model was built in Simulink. The parameters of main components of the new hydraulic luffing system can be seen in Table 3.

Figure 15 shows the step response of the new hydraulic luffing system for rescue vehicles. It can be seen that the response lag of the system arm lifting and descending were 0.1s and 0.08s respectively, and the steady-state errors were less than 0.001m/s, suggesting that the system had a high response speed and a low steady-state error.

To verify the servo performance of the system, the valve-controlled system's test speed v_s, after smoothing, was adopted as the input signal to analyze the dynamic performance of the new hydraulic luffing system for rescue vehicles. Figure 16 and Figure 17 respectively depict the speed tracking curve and the speed tracking error curve. It can be seen that the system could very satisfactorily track the input signal, and that the relatively significant tracking errors usually occurred in the switching control process of the speed increase from 0 or the speed reduction to 0, and the maximum error was less

than 0.0014m/s. The results indicated that the speed tracking system had a good servo performance.

Figure 18 depicts the control angle of the port plate. As can be seen from Figure 18, the control angle presented two significantly different change trends: in the time periods of 9.19s-9.34s, 20.74s-20.87s, 37.65s-37.73s, and 48.75s-48.86s, it adopted the control mode of switching preset control angle, and the control angle changed very quickly in these periods; with the transition of the control mode into FPID control, the change of the control angle gradually tended to be stabilized. Figure 19 and Figure 20 respectively

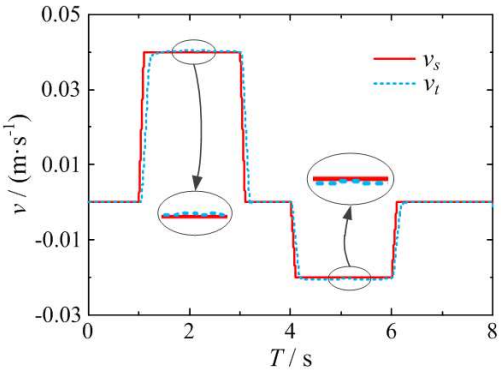

FIGURE 15. Step response of the new hydraulic luffing system

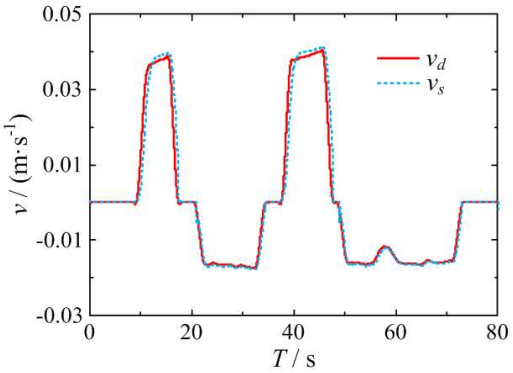

FIGURE 16. Speed tracking curve of the new hydraulic luffing system

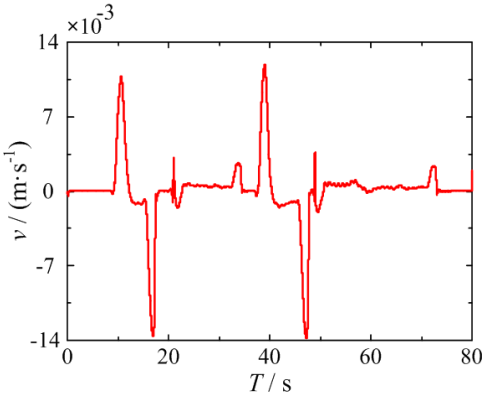

FIGURE 17. Speed tracking error of the new hydraulic luffing system

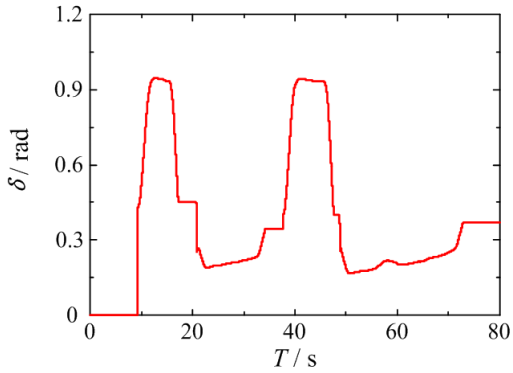

FIGURE 18. The control angle of the port plate

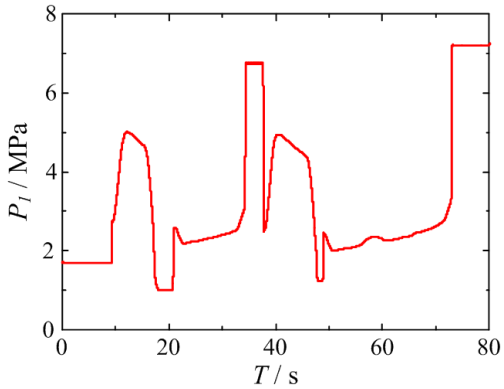

FIGURE 19. Pressure curve of the hydraulic cylinder's head port

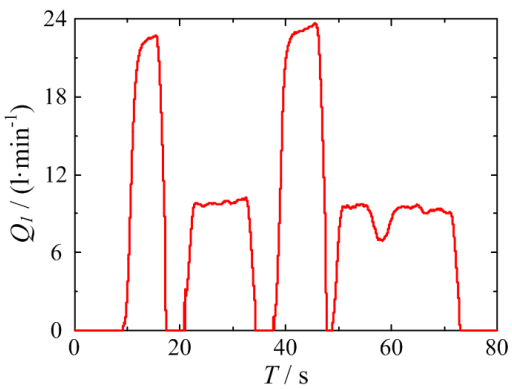

FIGURE 20. Flow curve of the hydraulic cylinder's head port

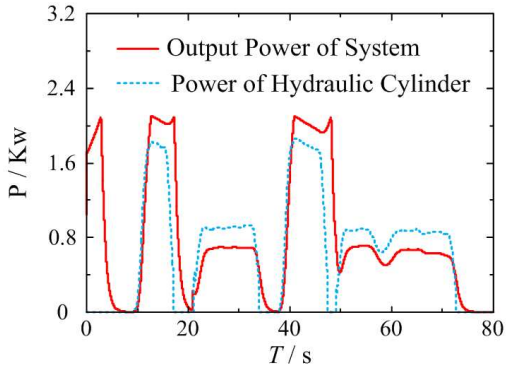

FIGURE 21. Output power of the new system and power curve of the hydraulic cylinder

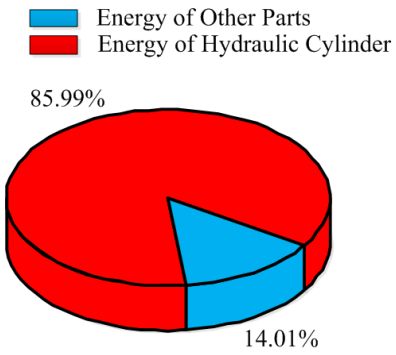

FIGURE 22. Proportion of effective energy consumption in the new system's total energy consumption

TABLE 4. The total energy consumption of new system and valve-controlled system

The energy consumption of valve-controlled system	The energy consumption of new system	Value	The energy utilization rate
356.58KJ	62.44KJ	294.14KJ	82.49%

depict the pressure curve and flow curve of the hydraulic cylinder's head port. As can be seen from their curves, when the input signal was 0, the flow of the head port was basically 0 and the pressure was kept steady; when there was an arm lifting or arm descending input signal, both the pressure and the flow were quickly regulated with the change of the input signal, and there was neither intense oscillation nor local overpressure. The results demonstrated the effectiveness of the control strategy combining both switching preset control angle and the FPID.

Figure 21 depicts the output power of the new hydraulic luffing system and the power curve of the hydraulic cylinder; Figure 22 depicts the proportion of effective energy consumption compared to the total energy consumption of the new hydraulic luffing system. The energy consumption comparison between the new hydraulic luffing system and the valve-controlled system can be seen in Table 4. As can be seen through comparison of Figure 5 and Figure 21, the hydraulic cylinders of the old and new systems had basically consistent power consumptions, suggesting that the new system bore a basically consistent system load when repeating the action of the valve-controlled system under the same working cycle. The new system had a maximum output power of only about 2Kw, between 21s-34s and 50s-72s in the cycle, that is, the output power of the system when the arm was descending was less than the power consumption of the hydraulic cylinder. It was mainly because of the positive effect of gravity on the hydraulic cylinder during the arm descending. In the period from 0-4s, the system had a relatively high output power, while the power consumption of the hydraulic cylinder was basically 0, mainly because the system actively charged oil to the hydraulic accumulator.

As can be seen from Figure 22, the effective energy consumption used to actuate the hydraulic cylinder accounted for as much as 85.99% of the total energy consumption of the system; relative to 11.82% for the valve-controlled system, the new system had a significantly increased energy utilization rate. According to Table 4, in the same cycle,

the valve-controlled system had a total energy consumption as high as 356.58KJ, while the new system had a total energy consumption of only 62.44KJ, so the energy-saving rate [28] had reached 82.49%. Thus, the new system could effectively reduce the energy consumption and increase the energy utilization rate.

7. **Conclusions and Future Work.** In this work, a new SHT-controlled hydraulic luffing system for rescue vehicles has been proposed to resolve the problems of the high energy consumption and low energy utilization rate of valve-controlled hydraulic luffing systems. And then a control strategy combining switching preset control angle and the FPID was also proposed to improve the dynamic performance of new system.

The new system could not only effectively follow the pressure and flow needed for a given load change to steadily complete the arm lifting and arm descending actions, but also significantly reduce the system's energy consumption and increase its energy utilization rate. The system did not produce any significant instantaneous pressure fluctuations or local overpressure when working, and there was no intense oscillation in the pressure or flow; the switching control process was very smooth, and the system demonstrated high flexibility. And the system had a quick dynamic response, a relatively high tracking precision and a good servo performance. For future work, the operating efficiency of the system will be analyzed and optimized, and related experiments will be conducted to further verify the effectiveness and feasibility of the system.

REFERENCES

[1] G. E. M. Vael, P. A. J. Achten and J. Potma, Cylinder control with the floating cup hydraulic transformer, *The 8th Scandinavian International Conference on Fluid Power*, 2003.
[2] W. Shen, H. Huang, Y. Pang et al., Review of the energy saving hydraulic system based on common pressure rail, *IEEE Access*, no.99, pp.1-23, 2017.
[3] S. Lee and P. Y. Li, Passivity based backstepping control for trajectory tracking using a hydraulic transformer, *ASME/BATH 2015 Symposium on Fluid Power and Motion Control*, 2016.
[4] J. Huang, Z. Dong, L. Quan et al., Development of a dual displacement controlled circuit for hydraulic shovel swing motion, *Automation in Construction*, no.57, pp.166-174, 2015.
[5] Y. X. Yu and K. K. Ahn, Application of hydraulic transformer on energy saving for boom system of hybrid hydraulic excavator, *Applied Mechanics & Materials*, no.868, pp.118-123, 2017.
[6] S. Lee and P. Li, A hardware-in-the-loop (HIL) testbed for hydraulic transformer research, *Scandinavian International Conference on Fluid Power*, 2017.
[7] E. M. V. Georges, A. J. A. Peter and F. Zhao, The Innas hydraulic transformer: The key to the hydrostatic common pressure rail, *SAE International Off-Highway and Powerplant Congress and Exhibition*, vol.21, no.1, pp.2561-2576, 2000.
[8] P. A. J. Achten, Z. Fu and G. E. M. Vael, Transforming future hydraulics: A new design of a hydraulic transformer, *Scandinavian International Conference on Fluid Power*, no.287, 1997.
[9] W. Wu, J. Hu, S. Yuan et al., A hydraulic hybrid propulsion method for automobiles with self-adaptive system, *Energy*, no.114, pp.683-692, 2016.
[10] W. Shen and J. Jiang, Analysis of energy recovery efficiency of hydraulic hybrid excavator, *Journal of South China University of Technology: Natural Science Edition*, vol.40, no.1, pp.82-87, 2012.
[11] J. F. Gaspar, M. Calvário, M. Kamarlouei et al., Power take-off concept for wave energy converters based on oil-hydraulic transformer units, *Renewable Energy*, no.86, pp.1232-1246, 2016.
[12] Y. Shi, Y. Wang, H. Liang et al., Power characteristics of a new kind of air-powered vehicle, *International Journal of Energy Research*, vol.40, no.8, pp.1112-1121, 2016.
[13] J. F. Gaspar, M. Kamarlouei, A. Sinha et al., Speed control of oil-hydraulic power take-off system for oscillating body type wave energy converters, *Renewable Energy*, no.97, pp.769-783, 2016.
[14] C. Liu, Y. Liu, J. Liu et al., Electro-hydraulic servo plate-inclined plunger hydraulic transformer, *IEEE Access*, no.99, pp.1-9, 2016.
[15] S. Liu and B. Yao, Coordinate control of energy saving programmable valves, *IEEE Trans. Control Systems Technology*, vol.16, no.1, pp.34-45, 2008.

[16] C. Guan and S. Pan, Adaptive sliding mode control of electro-hydraulic system with nonlinear unknown parameters, *Control Engineering Practice*, vol.16, no.11, pp.1275-1284, 2008.
[17] Y. Tang, H. Gao, W. Zou et al., Distributed synchronization in networks of agent systems with nonlinearities and random switchings, *IEEE Trans. Cybernetics*, vol.43, no.1, pp.358-370, 2013.
[18] Q. Q. Chen, M. H. Hung and F. Zou, Effective and adaptive algorithm for pepper-and-salt noise removal, *IET Image Processing*, vol.11, no.9, pp.709-716, 2017.
[19] W. Sun, H. Gao and B. Yao, Adaptive robust vibration control of full-car active suspensions with electrohydraulic actuators, *IEEE Trans. Control Systems Technology*, vol.21, no.6, pp.2417-2422, 2013.
[20] W. Shen, J. Jiang and K. Wang, Dynamic analysis of boom on hydraulic transformer, *Transactions of the Chinese Society for Agricultural Machinery*, vol.44, no.4, pp.27-32, 2013.
[21] W. Shen, J. Jiang, X. Su et al., A new type of hydraulic cylinder system controlled by the new-type hydraulic transformer, *ARCHIVE Proc. of the Institution of Mechanical Engineers Part C Journal of Mechanical Engineering Science 1989-1996 (vols 203-210)*, vol.228, no.12, pp.2233-2245, 2014.
[22] G. Yang and J. Jiang, Flow characteristics of variable hydraulic transformer, *Journal of Central South University*, vols.543-547, no.6, pp.741-746, 2015.
[23] H. Lu, J. Jiang, W. Zhang et al., Hydraulic transformer driving hydraulic cylinder based on constant-pressure hydraulic rail system, *Journal of Jilin University (Engineering and Technology Edition)*, vol.39, no.4, pp.885-890, 2009.
[24] R. Hippalgaonkar and M. Ivantysynova, Fuel savings of a mini-excavator through a hydraulic hybrid displacement controlled system, *International Conference on Fluid Power*, 2012.
[25] H. Moradi, H. Setayesh and A. Alasty, PID-fuzzy control of air handling units in the presence of uncertainty, *International Journal of Thermal Sciences*, no.109, pp.123-135, 2016.
[26] T. Mahto and V. Mukherjee, Fractional order fuzzy PID controller for wind energy-based hybrid power system using quasi-oppositional harmony search algorithm, *IET Generation Transmission & Distribution*, vol.11, no.13, pp.3299-3309, 2017.
[27] K. Kim and R. C. Schaefer, Tuning a PID controller for a digital excitation control system, *IEEE Trans. Industry Applications*, vol.41, no.2, pp.485-492, 2005.
[28] D. Zhao, M. Chen, Q. Dai et al., System of arm potential energy recovery in hybrid hydraulic excavators, *Journal of Jilin University (Engineering and Technology Edition)*, pp.150-154, 2011.